Cytokine Spätzle binds to the *Drosophila* immunoreceptor Toll with a neurotrophin-like specificity and couples receptor activation

Miranda Lewis[a], Christopher J. Arnot[a], Helen Beeston[b], Airlie McCoy[c], Alison E. Ashcroft[b], Nicholas J. Gay[a,1], and Monique Gangloff[a,1]

[a]Department of Biochemistry, University of Cambridge, Cambridge CB2 1GA, United Kingdom; [b]Astbury Centre for Structural Molecular Biology, University of Leeds, Leeds LS2 9JT, United Kingdom; and [c]Department of Haematology, University of Cambridge, Cambridge Institute for Medical Research, Cambridge CB2 0XY, United Kingdom

Edited by K. Christopher Garcia, Stanford University, Stanford, CA, and approved November 4, 2013 (received for review September 9, 2013)

Drosophila **Toll functions in embryonic development and innate immunity and is activated by an endogenous ligand, Spätzle (Spz). The related Toll-like receptors in vertebrates also function in immunity but are activated directly by pathogen-associated molecules such as bacterial endotoxin. Here, we present the crystal structure at 2.35-Å resolution of dimeric Spz bound to a Toll ectodomain encompassing the first 13 leucine-rich repeats. The cystine knot of Spz binds the concave face of the Toll leucine-rich repeat solenoid in an area delineated by N-linked glycans and induces a conformational change. Mutagenesis studies confirm that the interface observed in the crystal structure is relevant for signaling. The asymmetric binding mode of Spz to Toll is similar to that of nerve growth factor (NGF) in complex with the p75 neurotrophin receptor but is distinct from that of microbial ligands bound to the Toll-like receptors. Overall, this study indicates an allosteric signaling mechanism for Toll in which ligand binding to the N terminus induces a conformational change that couples to homodimerization of juxtamembrane structures in the Toll ectodomain C terminus.**

Toll receptor | Spz ligand | crystallography | mass spectrometry | isothermal titration calorimetry

Both *Toll* and *Spätzle* (*Spz*) were originally identified in screens that detected genes required for dorsoventral axis formation of *Drosophila melanogaster* embryos (1). Toll is a transmembrane receptor with a composite leucine-rich repeat (LRR) ectodomain, a single-span transmembrane region and an intracellular signaling domain, the Toll/Interleukin-1 receptor domain or TIR. Subsequently, Toll and Spz were shown to mediate antibacterial and antifungal responses in adult flies and larvae (2–5). A related family of molecules, the Toll-like receptors (TLRs), was later discovered in vertebrates, and these receptors also function in innate immunity (6–10). Unlike *Drosophila* Toll, which is activated by the endogenous ligand Spz, the TLRs are pattern-recognition receptors that respond directly to pathogen-associated molecules such as double-stranded RNA (11, 12). An exception to this mechanism of detection is TLR4, which requires the coreceptor MD-2 to recognize lipolysaccharides from Gram-negative bacteria (13).

Spz resembles mammalian growth factors and particularly the neurotrophin family, such as nerve growth factor (NGF). Spz is synthesized in an inactive form with a signal peptide that drives secretion, an N-terminal prodomain of varying size depending on the splicing process (14) and a C-terminal active fragment of 106 amino acids (C106). The latter adopts a dimeric cystine-knot (CK) structure, a fold very similar to that of NGF (15–19). Spz is activated by maternal signals or immune challenges that trigger specific protease cascades, stimuli that lead to endoproteolytic processing. Before cleavage, the prodomain is thought to mask the receptor-binding site by a mechanism reminiscent of the activation of the chymotrypsin zymogen and coagulogen, a clotting factor from the horseshoe crab (20). Activation-induced proteolysis causes a conformational change that exposes critical determinants for Toll binding on C106 that are masked by the prodomain before proteolysis (20). The prodomain is released from C106 upon Toll binding (21).

Previous biochemical studies suggest that initial activation of dToll, like the TLRs, requires ligand-induced dimerization of two receptor ectodomains (21–23). Ion mobility mass spectrometry and electron microscopy reveal that the full-length Toll ectodomain and Spz C106 form both 1:1 and 2:2 complexes although small amounts of a 2:1 stoichiometry can also be detected. This work also indicated that the binding site for Spz is located at the N terminus of the Toll ectodomain. Deletion mutations that truncate the ectodomain are constitutively active (24), and thus the ectodomain has an autoinhibitory function similar to that of vertebrate TLR4 (25). Binding of Spz relieves this inhibition, enabling homodimerization of the receptor and signaling to occur. Several lines of evidence suggest that the extracellular juxtamembrane region is directly involved in receptor homodimerization (24, 26, 27). For example, receptors with mutations of cysteine residues in the juxtamembrane capping structure are constitutively active, and the resultant unpaired cysteine forms intramolecular disulphide bonded dimers. In contrast to the TLRs, dToll signaling displays negative cooperativity so that the receptor responds over a wide range of ligand concentrations (reviewed in ref. 28).

In vertebrates, the neurotrophin family have essential developmental functions in neuronal survival, axon targeting, and connectivity and, in adult life, in learning, memory, and cognition

Significance

The ability of multicellular organisms to detect and respond to infection by microorganisms is fundamental and has ancient evolutionary origins. In mammals, immune system cells recognize danger molecules directly using "pattern recognition" receptors belonging to the Toll family among others. In insects, by contrast, Gram-positive bacteria and fungi can also be detected indirectly by an endogenous molecule, Spätzle (Spz), that activates related Toll receptors, leading to an effective immune response. In this study, we report the molecular structure of Spz/Toll complex, which reveals that Spz's mode of action is similar to neurotrophins, a family of proteins involved in the development and homeostasis of the insect and vertebrate nervous systems.

Author contributions: N.J.G. and M.G. designed research; M.L., C.J.A., H.B., and M.G. performed research; A.M. contributed new analytic tools; A.E.A., N.J.G., and M.G. analyzed data; and N.J.G. and M.G. wrote the paper.

The authors declare no conflict of interest.

This article is a PNAS Direct Submission.

Freely available online through the PNAS open access option.

Data deposition: The atomic coordinates and structure factors have been deposited in the Protein Data Bank, www.pdb.org (PDB ID code 4BV4).

[1]To whom correspondence may be addressed. E-mail: mg308@cam.ac.uk or njg11@cam.ac.uk.

This article contains supporting information online at www.pnas.org/lookup/suppl/doi:10.1073/pnas.1317002110/-/DCSupplemental.

(29). The NTs signal through three distinct receptors (NTRs)—$p75^{NTR}$, tyrosine receptor kinase (Trk), and Sortilin—and a shared downstream target is the activation of NFκB (30–32). Crystal structures are available for several complexes of vertebrate neurotrophins and their receptors that reveal distinct modes of binding and activation for different combinations of receptors and neurotrophins (33–36). In *Drosophila*, there are no canonical homologs of these receptors, but a recent study shows that the Toll and Spz paralogues (dToll6/7 and DNT1/2, respectively) fulfill these functions in the insect (37). This finding suggests that *Drosophila* Toll receptors may be mechanistically more similar to the vertebrate NTRs than to the TLRs. However, other studies show that dToll7 can also mediate antiviral responses to vesicular stomatitis virus and thus has a dual function in the nervous and immune systems (38).

To further understand the mechanism of Toll signaling, we crystallized and solved the structure of a complex of the Toll ectodomain and Spz. This structure reveals a mode of binding that is strikingly similar to that of NGF and $p75^{NTR}$ but different from that observed for the ligands of the mammalian TLRs. This arrangement suggests that ligand binding induces a secondary homodimerization of the receptor ectodomain and provides a molecular explanation for the observed negative allostery of the dToll signaling pathway.

Results

Overall Structure of a Partial Toll Ectodomain Bound to Spz C106. We present the crystal structure at 2.35-Å resolution of the N-terminal cap and first 13 LRRs of the ectodomain ($Toll_{N13}$–VLR) in complex with a Spz C106 dimer (Fig. 1). The receptor–ligand complex crystallized in space group C2 with one Spz C106 dimer and a single $Toll_{N13}$–VLR in the asymmetric unit.

The overall structure of $Toll_{N13}$–VLR adopts the shape of a curved solenoid that is relatively flat and binds Spz at its concave side within the first 10 LRRs (Fig. 1). The interface covers a total surface buried area of about 1,590 $Å^2$ (Table S1). There are 28 hydrogen bonds and 16 salt bridges that stabilize the complex on the concave side (Tables S2 and S3). Spz C106 interacts via its cystine-knot structure in an asymmetric binding mode that is reminiscent of the neurotrophin NGF bound to the receptor $p75^{NTR}$ (36). Like NGF, Spz forms an interface located at the "seam" of the ligand's dimeric structure, with each protomer contributing different epitopes to the complex. The proximal chain possesses a large continuous interface of 1,144 $Å^2$, which is over twice the size of the distal chain's interaction surface (533 $Å^2$) and displays two areas of contact centered around Q62 and Q74 that form hydrogen bonds with Toll residues from LRR6 and LRR7 and the cap, respectively. The cystine-knot protomers superimpose on each other with an rmsd of 1.2 Å over 390 atoms as a consequence of this asymmetry in contrast to 0.5 Å in the unbound structure of Spz. Binding to Toll distorts the cystine-knot structure as is also seen in NGF/$p75^{NTR}$ (36).

Ligand Binding Induces Conformational Changes in the Toll Ectodomain. We next investigated whether Spz induces conformational changes in the LRR solenoid of Toll. The first 201 residues of unbound Toll (39) and Spz C106 (19) were superimposed onto the corresponding regions of $Toll_{N13}$–VLR–Spz (Fig. 2). Toll leucine-rich repeat N-terminal domain (LRRNT) up to LRR6 (residues 28–228) superimposed with an rmsd of 0.9 Å over 1,240 atoms. The main shifts are observed in LRRNT in a region that also displayed high-temperature factors in the apo-structure. Upon ligand binding, residues from the N-terminal α-helix and adjacent loop are displaced by up to 4.6 Å for D40 and 3.6 Å for E61. The latter is involved in a salt bridge with Spz residue K15 in the complex structure whereas the former would clash with the wing of the distal Spz protomer at residues 80–86 if it adopted the same conformation as in the uncomplexed structure.

Spz Protrudes from the N-Terminal End of Toll. The cystine-knot structure of Spz displays very low B-factors in complex with Toll compared with its structure in isolation due to stabilization through numerous polar contacts (Tables S2 and S3). The structure solution with refolded Spz (19) as a template for molecular replacement, which does not account for the Trp loops, had C-alpha clashes in the wings and was rejected in the packing test. Only the cystine-knot structure could be assigned in the electron density of the crystal structure of the complex. Both the tryptophan loops (residues 19–40 in the proximal chain and residues 21–39 in the distal one) and the wings of Spz comprising the hairpin structures protruding between the first and the second strands (proximal residues 77–92 and distal ones 77–90) are invisible in the crystal structure. The missing Spz lobes are nevertheless physically present and intact as shown by SDS/PAGE analysis of

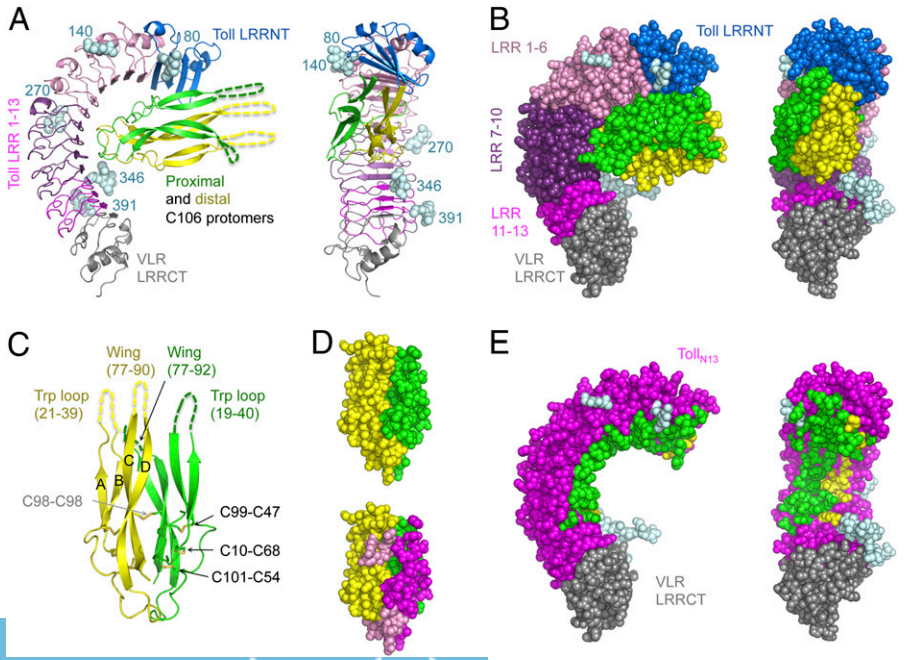

Fig. 1. Toll–Spz overall structure and ligand binding mode. (*A*) Schematic representation in two orientations (side view and concave view) with color-coded areas for Toll and Spz C106 dimer. The first *N*-acetylglucosamine residue of the glycan structures attached to Asn residues at positions 80, 140, 270, 346, and 391 is shown in light cyan spheres. (*B*) Space-filling models highlight the spatial restriction provided by the presence of the glycosylations. (*C*) Schematic representation of Spz C106 with the four-stranded antiparallel β-sheet labeled A–D and the two missing regions, the Trp loop, and the wing of each protomer indicated by dashed lines and corresponding missing residue numbers. The disulfide bonds of the cystine residues involved in the knot motif are shown along with the intermolecular bond involving Cys-98 of each chain. (*D*) Space-filling model of the Spz cystine-knot domain as observed in the complex structure, color-coded by polypeptide chain in *Upper*. In *Lower*, the same orientation highlights the footprint left by Toll across the dimeric surface of the ligand (interface colored in magenta for the proximal chain and pink for the distal one). (*E*) The asymmetry of the binding to Toll is represented by color-coding Toll residues that interact with Spz in either green or yellow depending on which chain that they contact.

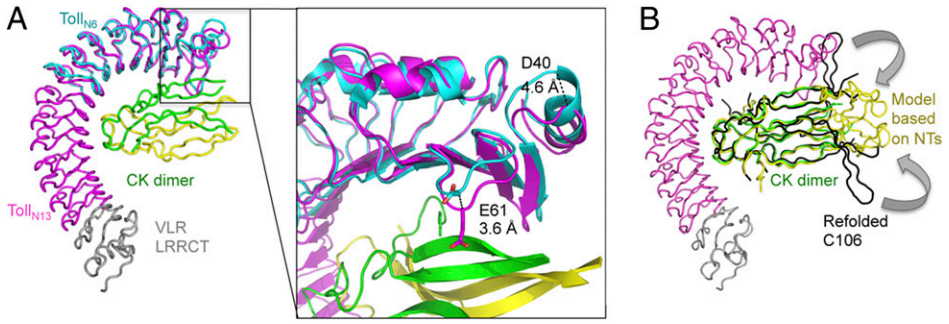

Fig. 2. Conformational changes induced by ligand binding and crystal packing. (*A*) Ribbon representation of Toll$_{N6}$ (residues 28–228 in cyan) superimposed on Toll$_{N13}$–VLR (magenta-gray) –Spz (green-yellow) reveals that conformational changes occur mainly in the Toll LRRNT region. The encapsulated close-up view shows a 4.6-Å shift of the Cα atom of D40 and a 3.6-Å shift for E61, which brings it in close proximity to Spz. (*B*) Ribbon representation of the Toll$_{N13}$–VLR–Spz complex superimposed on refolded Spz (black) (19) and a homology model of Spz based on NGF reveal steric hindrance by Toll LRRNT in the position of the wings. Arrows indicate potential repositioning of the wings.

dissolved crystals (Fig. S1). Moreover, the absence of electron density results in a gap in the crystal lattice in the region that would be occupied by these protrusions (Fig. S2).

We therefore tested different possible orientations of Spz's lobes by generating homology models based either on refolded Spz or on mammalian neurotrophins (NTs) (Fig. 2*B*). Using an NT-based model, both wings could be accommodated within the crystal lattice whereas the distal Trp loop clashed with the position of the VLR leucine-rich repeat C-terminal domain (LRRCT) of a symmetry-related receptor. Attempts to improve molecular models of this area using Phenix Morph (40) were not successful.

Mutagenesis of Spz Interface Residues. Next, we used site-directed mutagenesis to determine whether Spz residues in the binding interface are required for signal transduction. Mutants were expressed as TEV-cleavable constructs to facilitate the endoproteolytic processing required for activation of the ligand. To evaluate proper protein folding we verified the disulphide bonding patterns and protease resistance of the mutant proteins. The purified TEV-cleaved mutants were tested in an S2 cell culture assay, which measures the activation of a drosomycin promoter reporter construct (41).

A number of mutations that are surface-exposed failed to produce stable protein as judged by limited proteolysis with trypsin (R11E, L16A, N34A, N35A, and Q40R) or failed to purify on nickel columns (D26A, D27A, E85A, and D87A). On the other hand, the mutants R14A/K15A and D55R, located in different areas within the cystine-knot structure (Fig. 3*A*), were suitable for the S2-based signaling assay. The double mutant R14A/K15A changes two consecutive positively charged residues from the first beta-strand into alanines. R14 forms salt bridges with Toll E51 and E53 and a hydrogen bond with R66. The flexible side chain of K15 was modeled in alternative positions in which it is either involved in a salt bridge with E61 or in an H bond with the hydroxyl group at position 6 of the first *N*-acetyl-D-glucosamine (NAG) residue attached to N80 (Fig. 3*B*). The R14A/K15A mutation abolished signaling almost completely (Fig. 3*D*), which confirms the importance of this region for signaling and indicates a possible role of Toll glycosylation in ligand binding. We also tested a charge reversal mutation, D55R, chosen because an arginine is present at this position in mammalian NTs. This residue does not play a role in binding to TrkA, but, in proNGF and NT3, it forms a salt bridge with D134 of p75^{NTR} (Fig. S3). D55 is located in the loop following the second beta-strand of the cystine-knot structure, and the mutant Spz protein is severely defective in signaling (Fig. 3*C*).

The Toll/Spz Complex Resembles a Heterodimer of NGF and p75^{NTR}. In contrast to TLR4-MD-2 bound to the partial agonist lipid IVa (42) and TLR5 bound to flagellin (43), both of which are monomeric in solution but form into functional dimers upon crystallization, the crystal packing of Toll/Spz does not reveal a potentially relevant dimerization interface. The packing instead shows a ligand-mediated head-to-tail organization, an arrangement that could not be adopted by the full-length transmembrane receptor (Fig. S2). Modeling of a 2:1 Toll–Spz complex also proved impossible (Fig. S4). Indeed, the symmetrical binding surface on the other side of the ligand is not available for cross-linking a second Toll molecule because of steric hindrance between receptor chains, as is seen in some neurotrophin receptors. In fact, the Toll–Spz complex has remarkable similarity to the asymmetric dimer of NGF/p75NTR (36). On the other hand, the observed mode of binding is distinct to that seen with NGF and NT3 bound to the TrkA receptor (33–35) and the proNGF–p75^{NTR} complex (44), which are symmetrically cross-linked.

An array of techniques, including gel-filtration chromatography, analytical ultracentrifugation (AUC), and mass spectrometry

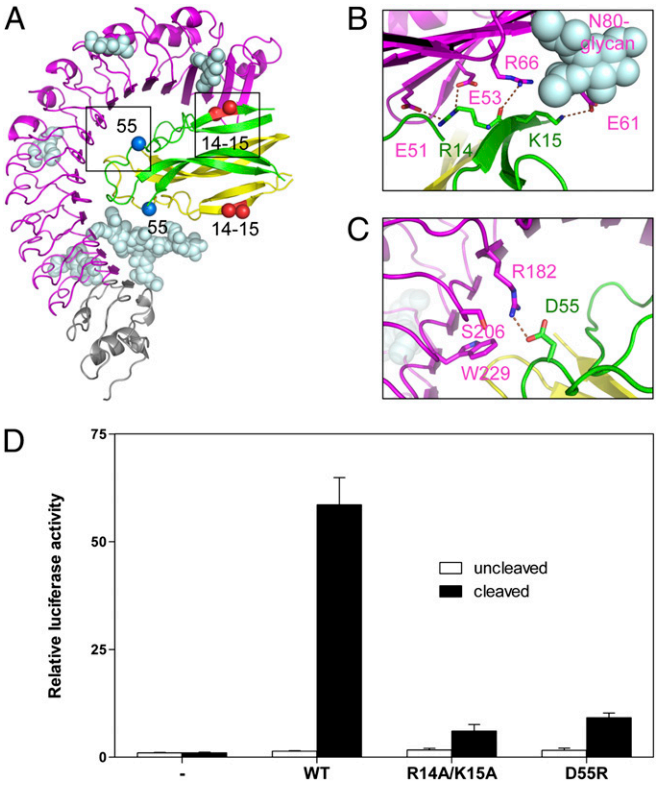

Fig. 3. Mutagenesis of Toll/Spz interface residues observed in the crystal structure. (*A*) Position in the interface of residues targeted for mutation: R14, K15, and D55 (boxed) and their symmetry-related counterpart on the other protomer. (*B* and *C*) Detailed views of the interactions between R14, K15, and D55 and the Toll ectodomain. (*D*) Spz mutants are defective in signaling. White bars indicate activity of 100 nM protein before protease cleavage and black bars after. Data are shown as relative luciferase induction and represented as mean ± SD (error bars).

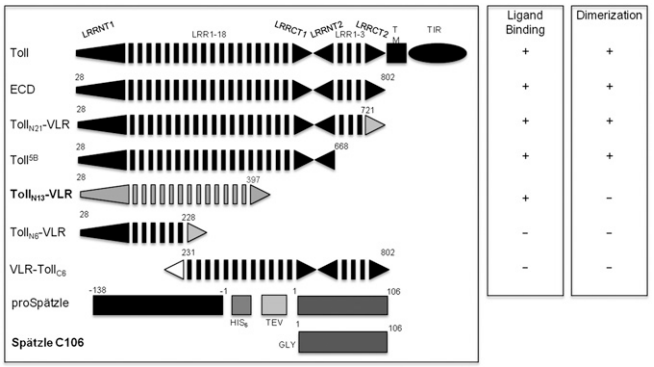

Fig. 4. Ligand-binding and dimerization abilities of Toll truncations. All constructs containing at least the N-terminal 399 residues are able to bind Spz C106 according to a range of biophysical techniques. White and gray triangles indicate VLR capping structures, black triangles native Toll N- and C-caps. The Spz construct is represented before and after TEV processing, which leaves an additional glycine residue at the N terminus of C106. The constructs Toll$_{N13}$–VLR and active Spz C106 have been used for crystallography.

unequivocally define the stoichiometry of the complex. Analytical gel filtration shows that Toll$_{N13}$–VLR is a monomer of 77 kDa and that the complex with Spz C106 is a heterodimer of 93 kDa. This conclusion is confirmed by AUC, experiments that also reveal that Toll$_{N13}$–VLR is heterogeneous (Fig. S5*B*). Mass spectrometry confirms that variable levels of glycosylation cause the observed heterogeneity.

Ligand Binding Is Required for Receptor Homodimerization. As ligand binding does not directly cross-link the receptor, we sought to identify regions of the Toll ectodomain required for dimerization using deletion mutagenesis (Fig. 4). We assessed the stoichiometry and Spz binding capacity of a number of N- and C- terminal truncations. We generated, among others, a construct called VLR–Toll$_{C6}$ that contained an N-terminal VLR capping structure (residues 1–82) (45) fused to the Toll ectodomain at the region C-terminal to LRR6 (residues 231–802). Interestingly, neither Toll$_{N6}$–VLR nor its C-terminally truncated counterpart VLR–Toll$_{C6}$, were able to form a stable complex with Spz, as shown by gel-filtration (Fig. S5*A*) although a small shift of elution position in the presence of Spz might indicate the formation of transient interactions, as reported previously. AUC and mass spectrometry analysis confirmed these data with the characterization of a heterogeneously glycosylated monomeric species of about 92 kDa and the absence of dimers (Fig. S5*C*). The properties of Toll$_{N6}$–VLR and VLR–Toll$_{C6}$ contrast with full-length Toll ectodomain and longer C-terminal truncations such as Toll^{5B}, which are able to bind ligand and to homodimerize (Fig. 4). Taken together, these data suggest that the N-terminal domain is required indirectly for dimerization of the receptor and formation of an active signaling complex.

We have also studied the stoichiometry and binding affinity of Spz for Toll$_{N13}$–VLR using isothermal titration calorimetry (ITC). In previous work, we carried out similar experiments using the full-length and Toll^{5B} ectodomain, experiments that revealed complex behavior (46). Specifically, different values of affinity and stoichiometry were obtained depending on whether the receptor or ligand was being titrated. By contrast, ITC experiments with Spz and Toll$_{N13}$–VLR produced a stoichiometry of 1:1 and an affinity of about 50 nM irrespective of which component was titrated (Fig. 5 and Table S4). Therefore unlike full-length Toll and Toll^{5B}, Toll$_{N13}$–VLR forms a simple bimolecular complex with Spz whereas full-length Toll and Toll^{5B} undergo secondary dimerization when Spz is bound.

Discussion

The crystal structure of the complex presented in this study defines the molecular basis of Toll and Spz recognition. The binding mode revealed in this high-resolution structure is significantly different from that proposed previously on the basis of electron microscopy (47). However, the quality and resolution (30 Å) of those images were poor, and the electron-density envelope defined could accommodate the arrangement revealed in this study. The structure is, however, consistent with our more recent study (39) that indicated that two discontinuous regions of interaction with the LRR solenoid are required for stable binding. In that study, mutagenesis of three residues in the N-terminal cap (C34, C43, and C45) led to only a partial reduction in Toll-signaling function. These residues do not interact with Spz although other cap residues, notably E61, do constitute a binding hot spot.

The binding mode of Spz observed in our structure is similar to that of mammalian NTs, particularly the NGF/p75^{NTR} complex as they share not only a similar asymmetric arrangement but also the same stoichiometry of one cystine-knot dimer for one receptor chain (36). As with full-length Toll/Spz, dimeric receptor complexes of NGF/ p75^{NTR} may also be formed in solution (48). The total buried surface area in the Toll–Spz complex is larger than that observed in neurotrophin receptor complexes. The binding surface is enclosed by glycan structures, one of which is found in direct contact with the ligand. Interestingly, receptor glycans also play important roles in NT binding, both by directly interacting with ligand and indirectly by determining the

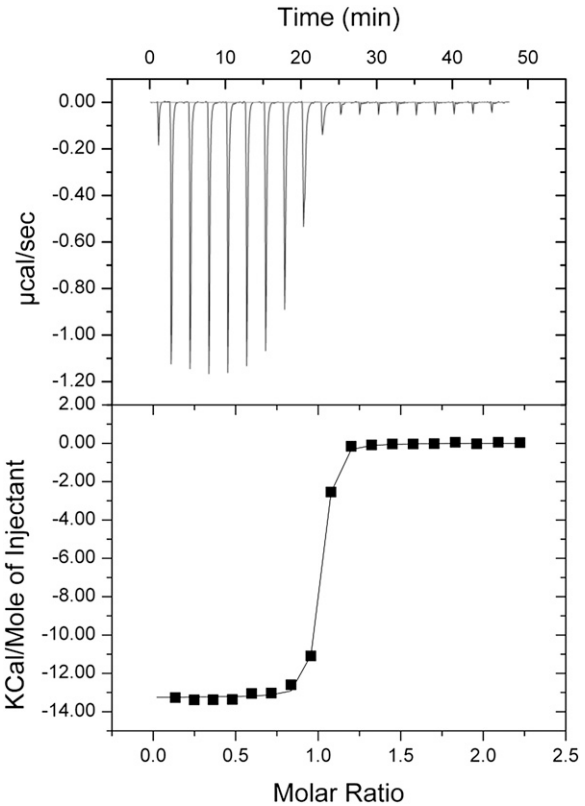

Fig. 5. Isothermal titration calorimetry of the Toll/Spz complex. Purified Spz C106 was titrated into the ITC measuring cell containing Toll$_{N13}$–VLR protein, which results in the formation of a complex of one truncated ectodomain binding a single Spz dimer with a dissociation constant between 30 and 50 nM, comparable with the affinity of full-length ectodomain. In the reciprocal titration in which Toll$_{N13}$–VLR was injected into Spz C106, a complex with the same stochiometry and dissociation constant was observed. A summary table of the thermodynamic parameters and a typical experiment is shown in Table S4.

correct conformation of the receptor (33–36). We also conclude that Spz binding cannot trigger receptor dimerization within a symmetrical 2:1 complex as is the case for NT-bound Trk receptor and proNGF or NT3-bound $p75^{NTR}$ because of major steric hindrance caused by the pronounced curvature of the Toll-receptor chains on the one hand (Fig. S3), and the concave binding mode of the cystine knot, on the other. It is likely that the 2:1 stoichiometry detected at low levels by mass spectrometry represents asymmetrically occupied receptor dimers present in trace amounts compared with major populations of 1:1 and 2:2 complexes (47).

In contrast to NTs whose structures have been described in free (49) and receptor-bound forms, Spz appears to be highly disordered both in its inactive form (22) and in complex with Toll. The Trp loops between the first and second β-strand and also the "wings" (the hairpin structure between the third and fourth strand of the cystine knot) are not resolved in the structure (Fig. 1). Both these protrusions that should be located at the top of the Spz dimer are not detected in electron density despite being intact and having enough space within the crystal lattice (Fig. S2). In the neurotrophins, the cystine knot is well defined, and only the prodomains are disordered. Although mature NGF signals via TrkA receptor to stimulate trophic functions, proNGF, like the TNF receptor, triggers $p75^{NTR}$ activity that leads to apoptosis. Interestingly, the prodomain regions in the crystal structure of the proNGF–$p75^{NTR}$ complex are mostly disordered whereas the wing structures have undergone conformational changes compared with mature NGF (44). Unlike proNGF, proSpz cannot bind Toll although it is conceivable that it can stimulate another receptor in *Drosophila* that is yet to be characterized. Previous studies have suggested flexibility in these regions of Spz C106 (19, 20). In particular, we showed that mutagenesis at the tryptophan residue W29F within the Trp loop did not affect Toll binding and activity whereas we established that it disrupted stable association between the Trp loop and the prodomain of unprocessed Spz (20). Thus, the Trp loop fulfills a negative regulatory role rather than being involved in binding to Toll. Moreover, we have shown that binding of processed Spz to the entire ectodomain of Toll leads to the dissociation of the prodomain (21). There is no experimental evidence to suggest that association of the prodomain with C106 following endoproteolytic cleavage of Spz has any functional consequences for signaling. Therefore, the role of the prodomain and the underlying mechanism of signaling differ significantly between NGF and Spz.

The *Drosophila* genome encodes nine Toll paralogues, but only Toll1, -7, and -8 are known to play a role in innate immunity. By contrast, the 11 human TLRs all function in immunity and respond by binding directly to pathogen-associated lipids, proteins, or nucleic acids. The interaction described here between Toll and Spz is significantly different from the ligand-binding modes of the Toll-like receptors, including protein binding to TLR4 (13, 45) and TLR5 (43). Whereas binding to Toll occurs at the concave surface of the LRR solenoid, binding of MD-2 to TLR4 and flagellin to TLR5 involves both concave and particularly the ascending lateral LRR surfaces. It is not clear whether the invisible lobes of Spz interact with Toll in the context of the full-length receptor. The mechanisms of TLR4 and TLR5 dimerization involve both ligand–receptor and receptor–receptor interactions in 2:2 complexes. Receptor dimerization occurs at ascending lateral and convex sides of the ectodomains that are either overlapping or downstream of the ligand-binding interface for TLR4 and TLR5, respectively. The comparison between the ligand binding and dimerization capacities of the constructs used for Toll and TLRs highlights common features as well as significant structural differences. For TLR4, residues 27–227 were sufficient for MD-2 binding but not dimerization (45). The truncations that were used in the structural characterization of TLR5 spanned over the LRRNT and the first 6, 12, and 14 LRRs, encompassing residues 22–181, 342, and 390, respectively. The first construct was too short to form a stable complex with its ligand flagellin, the second one bound flagellin but did not encompass the dimerization interface, and the third one, although monomeric in solution, adopted a tail-to-tail dimeric packing in the crystal structure. In the case of dToll, it is likely that binding of Spz at the N terminus induces a conformational change that enables a secondary homodimerization interface at the C terminus of the receptor ectodomain.

With the exception of Toll 9, the *Drosophila* Toll paralogues are more related to each other than they are to the TLRs. A recent study has shown that two of them, Toll6 and Toll7, fulfill the function of neurotrophin receptors in the insect nervous system (37). The ligands for Toll6 and -7 are two Spz paralogues called DNT1 and DNT2 (50). Toll6 and -7 are activated promiscuously by DNT1 and -2 and, like Toll1 and vertebrate neurotrophin receptors, signal activation of NFκB. Although there is considerable sequence divergence of Toll6/7 and DNT1/2 from Toll1 and Spz, it is likely that they signal by a similar molecular mechanism.

In previous work with full-length Toll ectodomain, we found that, even at high molar ratios of Spz, a mixture of 2:2 and 1:1 complexes is formed, a reflection of the observed negative allostery. We also used electron microscopy of negatively stained samples to reconstruct images of both 1:1 and 2:2 complexes (47). Although the resolution of these images is very low, they indicate the presence of receptor homodimerization interfaces at the juxtamembrane region and at the N terminus close to the Spz binding site, producing an overall configuration similar to that seen in the TLRs. In the present study, the Toll/Spz complex is a heterodimer, and we could find no evidence for homodimerization of the receptor, even in the crystal structure, which is a dense environment that can reinforce weak interactions as observed for TLR4 (42) and TLR5 (43). Taken together, the available data indicate that the N-terminal region is involved in an allosteric mechanism responsible for receptor dimerization at the C terminus.

To elucidate the molecular mechanism of negative cooperativity in Toll-Spätzle recognition, crystal structures of complexes with different stoichiometries are required. The strategy of receptor truncations is well suited for this purpose.

Methods

Generation of Toll Truncations. Toll–VLR constructs encompassing Toll residues 1–228 and 1–397, respectively, were generated as fusions with residues Asn-133 to Thr-201 of hagfish VLR B.61 by PCR. Toll truncations carried a 5′-BamHI and a 3′-NheI restriction site. The LRRCT of VLR B6.1 was generated with a 5′-NheI and a 3′-AgeI cloning site. The Fc domain of human IgG1 was amplified with a 5′-AgeI site followed by a TEV cleavage site and 3′-NotI site. Primers are listed in the Table S5. The Toll, VLR, and Fc fragments were digested with the corresponding restriction enzymes. The three products were then ligated to form a single Toll–VLR–Fc insert that was introduced into the BamHI and NotI sites of the pFastBac-1 transposition vector (Bac-to-Bac; Invitrogen).

Protein Expression and Purification. Fc-tagged Toll N-terminal truncations and His-tagged Spz were produced in a baculovirus expression system. The procedure for Spz preparation has been described elsewhere (21). Toll–VLR constructs were expressed in Sf9 insect cells (Invitrogen). The supernatant was collected by centrifugation 3 d after infection and concentrated using the Centramate tangential flow filtration system (Pall Filtron). It was loaded onto HiTrap protein A HP column (GE Healthcare). Purified protein was eluted in 0.1 M sodium citrate, pH 3.0. The Fc fusion was cleaved with TEV protease (51). The digestion products were separated by protein A affinity chromatography. Toll–VLR constructs were further purified by size-exclusion chromatography in 100 mM NaCl, 20 mM Tris·HCl, pH 7.0.

Crystallization of $Toll_{N13}$–VLR–C106 Complex. Both proteins were produced in a lepidopteran expression system and thus have near native N-linked glycosylation (52). Enzymatic deglycosylation was not required. Crystals were obtained with the vapor diffusion method in 15% PEG 8000, 0.1 M Tris pH 7.5, 0.1 M $MgCl_2$, with protein concentration of 4.7 mg/mL. Five weeks later, crystals were sequentially soaked in 10%, then 20% glycerol cryoprotectant solution and mounted in 20-μm nylon cryoloops (Hampton Research) before being immersed in liquid nitrogen for storage and diffraction. Crystals

belong to the space group monoclinic C2. The structure was determined by molecular replacement using as templates structural models for Spz (19) and Toll derived from a shorter truncation $Toll_{N6}$–VLR (39) along with homology models for the extra seven LRRs. The structure has been deposited in the Protein Data Bank with the PDB ID code 4BV4. See *SI Methods* for further details and Table S6 for X-ray diffraction data collection and refinement statistics.

Site-Directed Mutagenesis. Site-directed mutagenesis was performed using the QuikChange II kit (Stratagene). The primers are listed in Table S5. The mutagenized inserts were sequenced and then recloned into fresh pcDNA3.1 (+) or pFastBac-1 backbones. Mutations did not affect protein expression levels as assessed by Western blot detection.

ACKNOWLEDGMENTS. We thank Dr. Martin Moncrieffe, Dr. Gerhard Fischer, Dr. Katherine Stott, Dr. Dimitri Chirgadze, and the staff at the Diamond Light Source I24 beamline, England, for their assistance. This work was financed by programme grants from the Wellcome Trust (WT081744/Z/06/Z) and the United Kingdom Medical Research Council (G1000133) (to N.J.G.). The LCT Premier was purchased with funding from a Wellcome Trust Equipment Grant (WT 075099/Z/04/Z). H.B. is supported by a grant from the Biotechnology and Biological Sciences Research Council (BB/F01614/X).

1. Anderson KV, Bokla L, Nüsslein-Volhard C (1985) Establishment of dorsal-ventral polarity in the Drosophila embryo: The induction of polarity by the Toll gene product. *Cell* 42(3):791–798.
2. Lemaitre B, Nicolas E, Michaut L, Reichhart JM, Hoffmann JA (1996) The dorsoventral regulatory gene cassette spätzle/Toll/cactus controls the potent antifungal response in Drosophila adults. *Cell* 86(6):973–983.
3. Rosetto M, Engström Y, Baldari CT, Telford JL, Hultmark D (1995) Signals from the IL-1 receptor homolog, Toll, can activate an immune response in a Drosophila hemocyte cell line. *Biochem Biophys Res Commun* 209(1):111–116.
4. Shia AK, et al. (2009) Toll-dependent antimicrobial responses in Drosophila larval fat body require Spätzle secreted by haemocytes. *J Cell Sci* 122(Pt 24):4505–4515.
5. Kaneko T, et al. (2004) Monomeric and polymeric gram-negative peptidoglycan but not purified LPS stimulate the Drosophila IMD pathway. *Immunity* 20(5):637–649.
6. Rock FL, Hardiman G, Timans JC, Kastelein RA, Bazan JF (1998) A family of human receptors structurally related to Drosophila Toll. *Proc Natl Acad Sci USA* 95(2):588–593.
7. Medzhitov R, Preston-Hurlburt P, Janeway CA, Jr. (1997) A human homologue of the Drosophila Toll protein signals activation of adaptive immunity. *Nature* 388(6640):394–397.
8. Poltorak A, et al. (1998) Defective LPS signaling in C3H/HeJ and C57BL/10ScCr mice: Mutations in Tlr4 gene. *Science* 282(5396):2085–2088.
9. Janeway CA, Jr., Medzhitov R (2002) Innate immune recognition. *Annu Rev Immunol* 20:197–216.
10. Akira S, Uematsu S, Takeuchi O (2006) Pathogen recognition and innate immunity. *Cell* 124(4):783–801.
11. Liu L, et al. (2008) Structural basis of toll-like receptor 3 signaling with double-stranded RNA. *Science* 320(5874):379–381.
12. Kang JY, Lee JO (2011) Structural biology of the Toll-like receptor family. *Annu Rev Biochem* 80:917–941.
13. Park BS, et al. (2009) The structural basis of lipopolysaccharide recognition by the TLR4-MD-2 complex. *Nature* 458(7242):1191–1195.
14. DeLotto Y, Smith C, DeLotto R (2001) Multiple isoforms of the Drosophila Spätzle protein are encoded by alternatively spliced maternal mRNAs in the precellular blastoderm embryo. *Mol Gen Genet* 264(5):643–652.
15. Morisato D, Anderson KV (1994) The spätzle gene encodes a component of the extracellular signaling pathway establishing the dorsal-ventral pattern of the Drosophila embryo. *Cell* 76(4):677–688.
16. Schneider DS, Jin Y, Morisato D, Anderson KV (1994) A processed form of the Spätzle protein defines dorsal-ventral polarity in the Drosophila embryo. *Development* 120(5):1243–1250.
17. DeLotto Y, DeLotto R (1998) Proteolytic processing of the Drosophila Spätzle protein by easter generates a dimeric NGF-like molecule with ventralising activity. *Mech Dev* 72(1-2):141–148.
18. Mizuguchi K, Parker JS, Blundell TL, Gay NJ (1998) Getting knotted: A model for the structure and activation of Spätzle. *Trends Biochem Sci* 23(7):239–242.
19. Hoffmann A, et al. (2008) Biophysical characterization of refolded Drosophila Spätzle, a cystine knot protein, reveals distinct properties of three isoforms. *J Biol Chem* 283(47):32598–32609.
20. Arnot CJ, Gay NJ, Gangloff M (2010) Molecular mechanism that induces activation of Spätzle, the ligand for the Drosophila Toll receptor. *J Biol Chem* 285(25):19502–19509.
21. Weber AN, et al. (2007) Role of the Spatzle Pro-domain in the generation of an active toll receptor ligand. *J Biol Chem* 282(18):13522–13531.
22. Weber AN, et al. (2003) Binding of the Drosophila cytokine Spätzle to Toll is direct and establishes signaling. *Nat Immunol* 4(8):794–800.
23. Sun H, Towb P, Chiem DN, Foster BA, Wasserman SA (2004) Regulated assembly of the Toll signaling complex drives Drosophila dorsoventral patterning. *EMBO J* 23(1):100–110.
24. Winans KA, Hashimoto C (1995) Ventralization of the Drosophila embryo by deletion of extracellular leucine-rich repeats in the Toll protein. *Mol Biol Cell* 6(5):587–596.
25. Panter G, Jerala R (2011) The ectodomain of the Toll-like receptor 4 prevents constitutive receptor activation. *J Biol Chem* 286(26):23334–23344.
26. Schneider DS, Hudson KL, Lin TY, Anderson KV (1991) Dominant and recessive mutations define functional domains of Toll, a transmembrane protein required for dorsal-ventral polarity in the Drosophila embryo. *Genes Dev* 5(5):797–807.
27. Hu X, Yagi Y, Tanji T, Zhou S, Ip YT (2004) Multimerization and interaction of Toll and Spätzle in Drosophila. *Proc Natl Acad Sci USA* 101(25):9369–9374.
28. Gay NJ, Gangloff M, Weber AN (2006) Toll-like receptors as molecular switches. *Nat Rev Immunol* 6(9):693–698.
29. Lu B, Pang PT, Woo NH (2005) The yin and yang of neurotrophin action. *Nat Rev Neurosci* 6(8):603–614.
30. Gutierrez H, Davies AM (2011) Regulation of neural process growth, elaboration and structural plasticity by NF-κB. *Trends Neurosci* 34(6):316–325.
31. Foehr ED, et al. (2000) NF-kappa B signaling promotes both cell survival and neurite process formation in nerve growth factor-stimulated PC12 cells. *J Neurosci* 20(20):7556–7563.
32. Carter BD, et al. (1996) Selective activation of NF-kappa B by nerve growth factor through the neurotrophin receptor p75. *Science* 272(5261):542–545.
33. Gong Y, Cao P, Yu HJ, Jiang T (2008) Crystal structure of the neurotrophin-3 and p75NTR symmetrical complex. *Nature* 454(7205):789–793.
34. Wehrman T, et al. (2007) Structural and mechanistic insights into nerve growth factor interactions with the TrkA and p75 receptors. *Neuron* 53(1):25–38.
35. Wiesmann C, Ultsch MH, Bass SH, de Vos AM (1999) Crystal structure of nerve growth factor in complex with the ligand-binding domain of the TrkA receptor. *Nature* 401(6749):184–188.
36. He XL, Garcia KC (2004) Structure of nerve growth factor complexed with the shared neurotrophin receptor p75. *Science* 304(5672):870–875.
37. McIlroy G, et al. (2013) Toll-6 and Toll-7 function as neurotrophin receptors in the Drosophila melanogaster CNS. *Nat Neurosci* 16(9):1248–1256.
38. Nakamoto M, et al. (2012) Virus recognition by Toll-7 activates antiviral autophagy in Drosophila. *Immunity* 36(4):658–667.
39. Gangloff M, Arnot CJ, Lewis M, Gay NJ (2013) Functional insights from the crystal structure of the N-terminal domain of the prototypical toll receptor. *Structure* 21(1):143–153.
40. Adams PD, et al. (2010) PHENIX: A comprehensive Python-based system for macromolecular structure solution. *Acta Crystallogr D Biol Crystallogr* 66(Pt 2):213–221.
41. LeMosy EK, Tan YQ, Hashimoto C (2001) Activation of a protease cascade involved in patterning the Drosophila embryo. *Proc Natl Acad Sci USA* 98(9):5055–5060.
42. Ohto U, Fukase K, Miyake K, Shimizu T (2012) Structural basis of species-specific endotoxin sensing by innate immune receptor TLR4/MD-2. *Proc Natl Acad Sci USA* 109(19):7421–7426.
43. Yoon SI, et al. (2012) Structural basis of TLR5-flagellin recognition and signaling. *Science* 335(6070):859–864.
44. Feng D, et al. (2010) Molecular and structural insight into proNGF engagement of p75NTR and sortilin. *J Mol Biol* 396(4):967–984.
45. Kim HM, et al. (2007) Crystal structure of the TLR4-MD-2 complex with bound endotoxin antagonist Eritoran. *Cell* 130(5):906–917.
46. Weber AN, Moncrieffe MC, Gangloff M, Imler JL, Gay NJ (2005) Ligand-receptor and receptor-receptor interactions act in concert to activate signaling in the Drosophila toll pathway. *J Biol Chem* 280(24):22793–22799.
47. Gangloff M, et al. (2008) Structural insight into the mechanism of activation of the Toll receptor by the dimeric ligand Spätzle. *J Biol Chem* 283(21):14629–14635.
48. Aurikko JP, et al. (2005) Characterization of symmetric complexes of nerve growth factor and the ectodomain of the pan-neurotrophin receptor, p75NTR. *J Biol Chem* 280(39):33453–33460.
49. McDonald NQ, et al. (1991) New protein fold revealed by a 2.3-A resolution crystal structure of nerve growth factor. *Nature* 354(6352):411–414.
50. Zhu B, et al. (2008) Drosophila neurotrophins reveal a common mechanism for nervous system formation. *PLoS Biol* 6(11):e284.
51. Kapust RB, et al. (2001) Tobacco etch virus protease: Mechanism of autolysis and rational design of stable mutants with wild-type catalytic proficiency. *Protein Eng* 14(12):993–1000.
52. Jarvis DL, Finn EE (1995) Biochemical analysis of the N-glycosylation pathway in baculovirus-infected lepidopteran insect cells. *Virology* 212(2):500–511.